Characterization of a Time-of-Flight Camera for Use in Diffuse Optical Tomography

A thesis submitted in partial fulfillment of the requirements for the degree of Bachelor of Science degree in Physics from the College of William and Mary

by

Neal Parker

Advisor: Dr. William Cooke

Senior Research Coordinator: Henry Krakauer

Date: April 22, 2016

Introduction

Diffuse optical tomography is the use of diffuse light to create an image of the desired target. In our case, the CamBoard pico^s is a scanner-less LIDAR imager that uses an RF- modulated light source, being sinusoidally modulated at f_m = 30MHz $(s(t) = \sin(2\pi f_m))$. This time-of-flight camera sends out a pulse of 850nm light, illuminating the entire scene. The camera simply uses the difference in time between the outgoing and incoming light to determine the distance traveled ($r = \frac{2d}{c}$). The saturation of each pixel in the 21120 (176x120) pixels that are available is used to determine the spatial orientation of the arriving photons. So, when coupled with the distance information, an image can be constructed. This camera captures four images within every frame to create an image where the first and third and the second and fourth images collected are 90° out of phase.

There has been considerable focus on the prospects of using diffuse optical tomography as an alternative imaging technology in the health/veterinary fields as a low cost, much less invasive, more accessible, portable procedure when compared to MRI and CAT scans. This technology can be used to reconstruct images of biological tissues through solving the diffusion equation:

$$\frac{\partial \phi(r,t)}{\partial t} = \nabla \cdot [D(r) \cdot \nabla \phi(r,t)] - v\mu_a(r)\phi(r,t) + vS(r,t)$$

Where $\phi(r,t)$ is the photon fluence at location *r* and time *t*, $D(r)$ is the diffusion constant at location *r*, *v* is the speed of light in the material, and $S(r,t)$ is an isotropic source term. When the light, in the IR range, interacts with tissues of interest, some of the light enters the tissue and some is reflected. The light has some transit time for which it remains within the tissue before being reemitted. Analysis of the light that reemitted, while excluding the reflected incident light, allows one to render an image of the internal structure of the target region. This is typically done with one source and multiple detectors that are equidistant from that source. This has been used to do basic analysis of brain activity and is the basic idea behind pulse oximetry. Because vessels containing larger amounts of oxygenated hemoglobin absorb light differently than those containing a larger concentration of deoxygenated hemoglobin, analysis of the intensity of light being reemitted can be used to determine regions of the brain that are active during certain tasks [1]. This phenomenon of the absorbance shift of hemoglobin in its oxygenated and deoxygenated form is known as the BOLD effect (the Blood- Oxygen-Level Dependent effect).

Figure 1:The BOLD Effect [2]

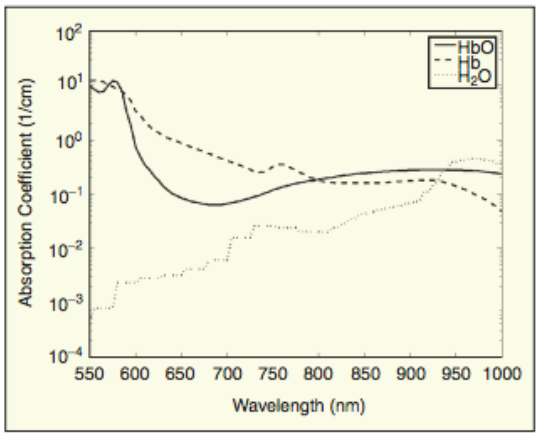

There are considerable issues associated with diffuse optical tomography, namely, that signal strength attenuates very rapidly. The light does not penetrate very far into the tissue meaning that the information collected is restricted to the periphery of the tissue. Complex geometry of tissues, distribution of tissues that have different coefficients of

absorption, potentially non-linear absorption, as well as thermal interference combine to further complicate the effort.

When compared to the "traditional" method of diffuse optical tomography, the method that we are exploring with the CamBoard pico^{s} would use a much greater density of detectors with each pixel acting as an individual detector. There are 120x176 pixels for just one source. This should allow for significantly greater resolutions of images acquired from tissues. However, because of the greater density of detectors compared to the number of sources, the strength of signal being provided to each detector would be reduced. I will be exploring this trade-off. If the efficiency of this dense array of detectors is too low, then this camera will not be useable for diffuse optical tomography.

Results

The CamBoard pico^{s} can exclude information from pixels where the amplitude of received light is too low, the detectors are being saturated, and/or the variation between pixels of a given region in the phase plot exceeds some value. I have gathered images, developed from phase and amplitude data from the camera, of a flat plane 30cm from the face of the camera. There are three main regions of interest here: the sides (left and right of the plane) that appear black and the plane itself.

Figures 2 and 3: Phase(left) and Amplitude(Right) Images of Flat Plane

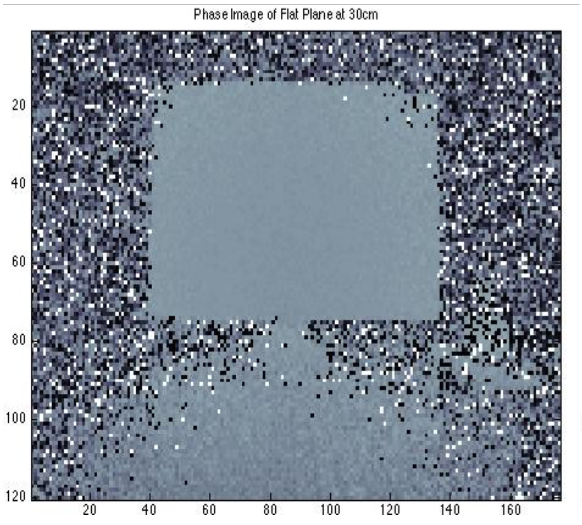

This image of a flat plane is generated solely from the phase information generated by the camera. There is little variation in the plane region compared to the non-plane regions surrounding the plane. This relative uniformity is a factor in determining the quality of data. Additionally, there are "rings of phase" within this plane region corresponding to different straight-line distances from the camera. (These rings will be more easily viewed in later images.)

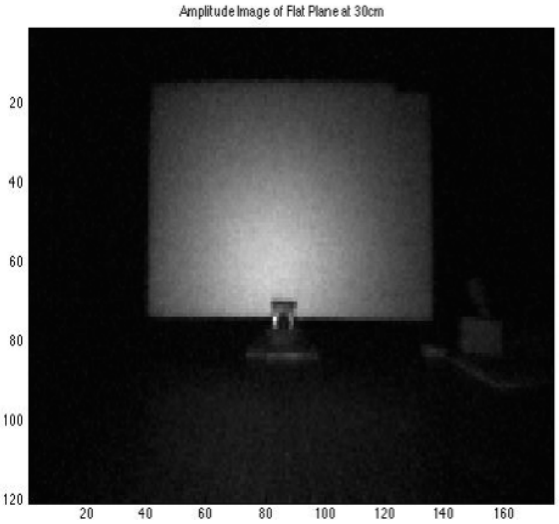

This image is generated from the amplitude data from the camera. You may notice that the location of much higher intensity striking the board. This is because the light from the camera striking this section of the board returns with considerably less photon loss than the others. The light in this region will show up as the region on the phase map with the smallest variation in phase.

Smaller boxes of increasing size within the plane and non-plane regions were selected and the standard deviation of the phase values within these smaller boxes was found and plotted against the area of each corresponding box to estimate the overall

standard deviation of each region. As the area of the boxes got larger and larger, the corresponding standard deviations converged on the population standard deviation of each region.

Figure 4: Estimation of Std. Deviation in Plane Region

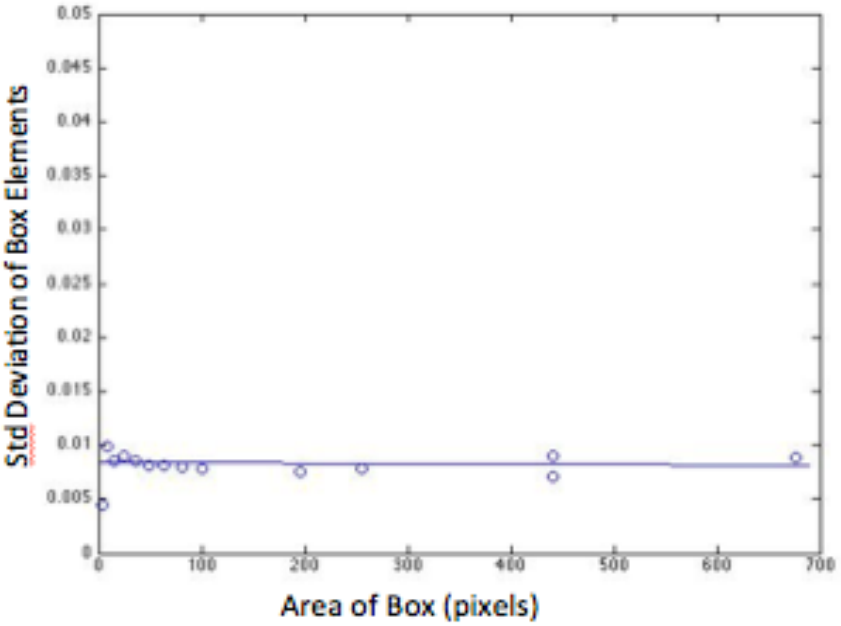

The above image shows the approximation of the true standard deviation of the phase within the plane region. The value of which was found to be .008 rad.

Figure 5: Comparison of Std. Deviations in Plane and Non-plane Regions

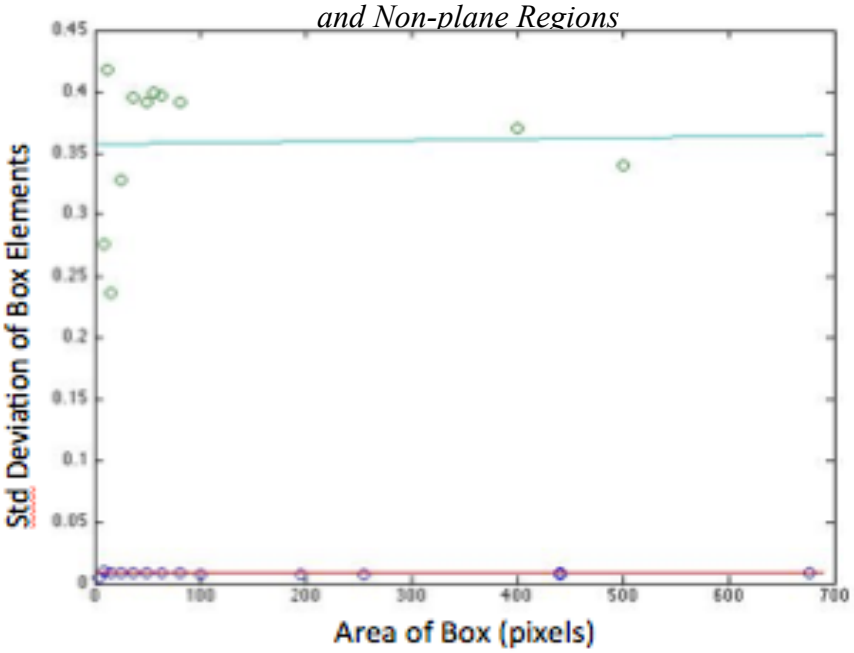

This figure shows a side-by-side comparison of the approximate standard deviations of the plane and non-plane regions. The value of the standard deviation in non-plane region was estimated to be .35 rad. This value likely undershoots the true value, as the two larger box sizes (500 and 400 pixels) seem to be outliers.

In general, the standard deviations of the phase in the dark regions are much greater than those in the plane region. Combining the information from the approximation of the true standard deviation of each region with the magnitude of the phase difference, allows us to see that one of the determining factors that the CamBoard software uses in determining "good vs. bad" image regions is the standard deviation in the phase of regions of pixels, not the magnitude of the phase. From the small samples I used, the average of the standard deviations in the plane region was .008 rad. While in the dark region, it was .3484 rad.

Figures 6:Magnitude of Phase Across One Row

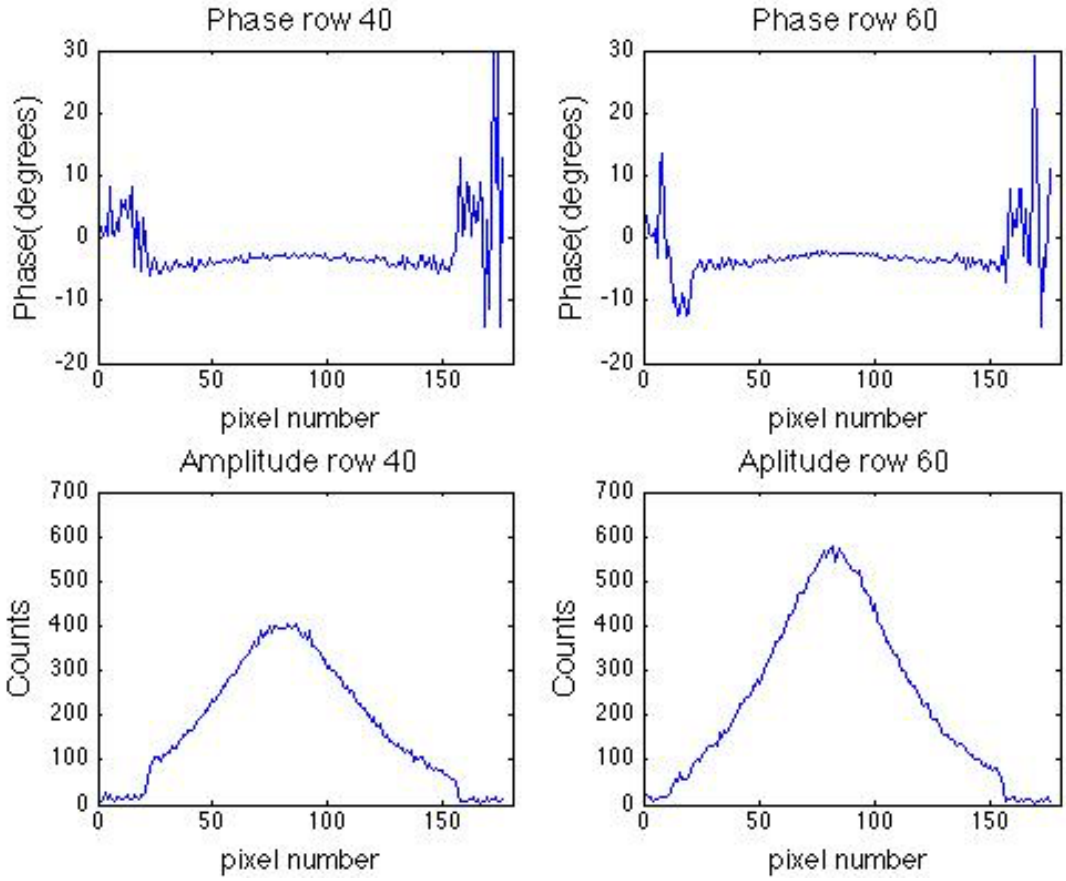

These rows were selected to show the variation in the phase values across one row of the phase image, which included points in the plane and non-plane regions. As you cans see, the regions with the highest amplitude corresponded to those with the least variation in phase. The highest amplitude corresponds to the shortest distance traveled by the light striking the plane. As you can see, there is slight warping that occurs through the middle of the phase plots. This is because the straight-line distance to the camera changes as you make your way across one row of pixels.

Another aspect of the project was to redirect the camera's light source using a fiber optic to obtain images of backlit synthetic fat. Roughly 16% of the original output of the camera's LED was diverted into the fiber. From there, two lenses, one with a focal length of 10cm and the other with a focal length of 4.5cm (figure 8), were used to

magnify the source and the object being imaged, the magnification being roughly 2x. The solid angle of the incident light would also increase; more light would strike the diode of the camera. Because of this, several neutral density filters had to be added between the camera and the second lens to keep from saturating the camera's detectors (Figure 8.)

Figure 7:Magnified Image of Wires

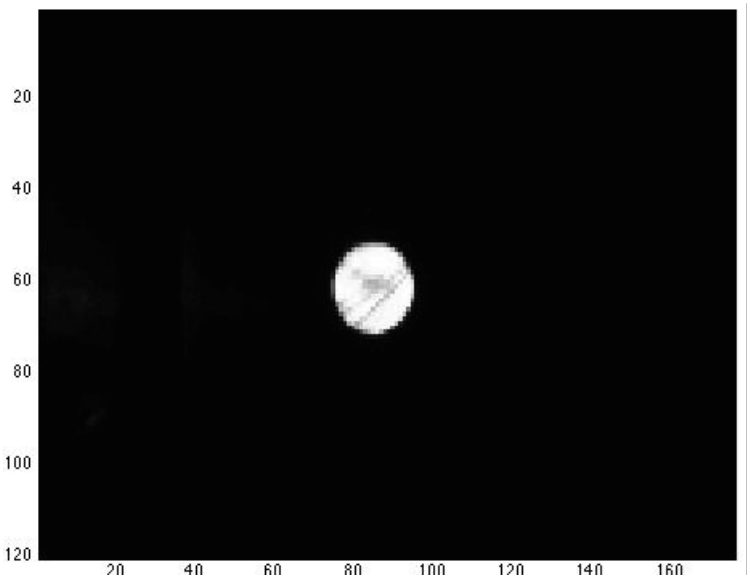

The above image is of small wires magnified and imaged by the CamBoard pico^{s} . These were viewed from a distance of 30cm. Each wire is ~.25mm in diameter.

Figure 8: Magnification Setup Used

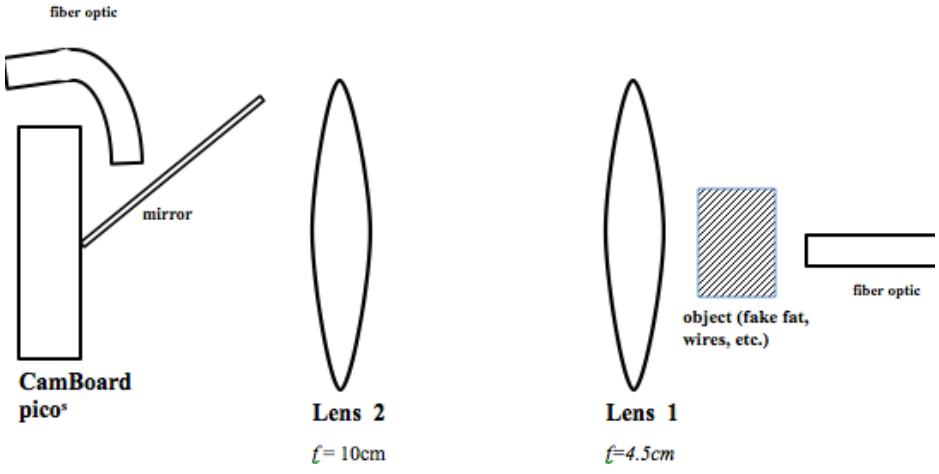

To determine if the CamBoard pico[s] would be a reliable detector to use for diffuse optical tomography, we must determine if the amount of photons incident to each detector (pixel) is sufficient for our uses. Because there is such a high density of detectors compared to the normal methods of diffuse optical tomography, it means that the amount of light incident to each would be considerably less. The camera shoots 45fps.

Figure 9: Image showing the shots taken per frame by the CamBoard

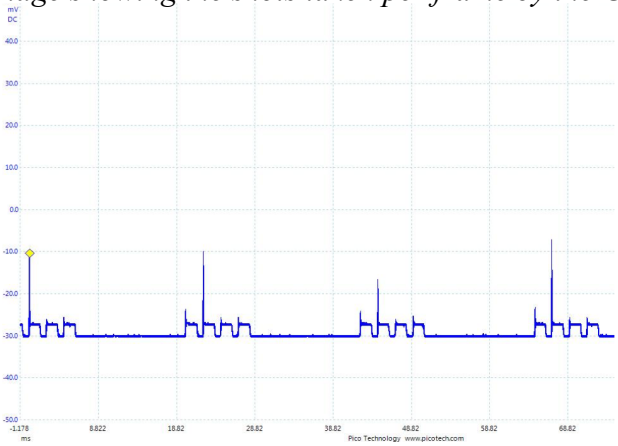

Each frame is made up of four individual shots corresponding to four different phases. These four images are then used to create one final image. During each of the four shots, the diode is rapidly turned on and off at 30MHz. In short, the diode is off for much more time than it is on. This means that the peak power emitted is higher than the measured average power. The average power was measured at a distance of 30cm from the camera.

$$avg\ power = 77\mu W$$

$$duty\ cycle = .41$$

$$P_{peak} = \frac{avg\ power}{duty\ cycle} = .000183W$$

With the camera set to an integration time of 1000μs, for one frame of four shots, the camera has emitted $1.83\text{x}10^{-7}$ J. This means that $7.82\text{x}10^{11}$ photons at 850nm have been emitted from the camera.

$$.000183W \times 1000\mu s = 1.83\text{x}10^{-7}\ \text{J}$$

$$E_{850} = 2.34\times10^{-19}J/photon$$

$$\frac{1.83\text{x}10^{-7}\ \text{J}}{2.34\times10^{-19}J/\ photon} = 7.82\times10^{11}\text{photons}$$

At a distance of .371 m between the plane and the camera, 330 counts were measured in the highest region of amplitude. This was measured using LightVis. The area contained in the image was determined by measuring height and width of the area of the board that could be seen on the phase image in the LightVis application. Once the light strikes the plane, it is reflected back into an angle of roughly 1sr (this was tough to measure).

Simple sketch showing the camera setup

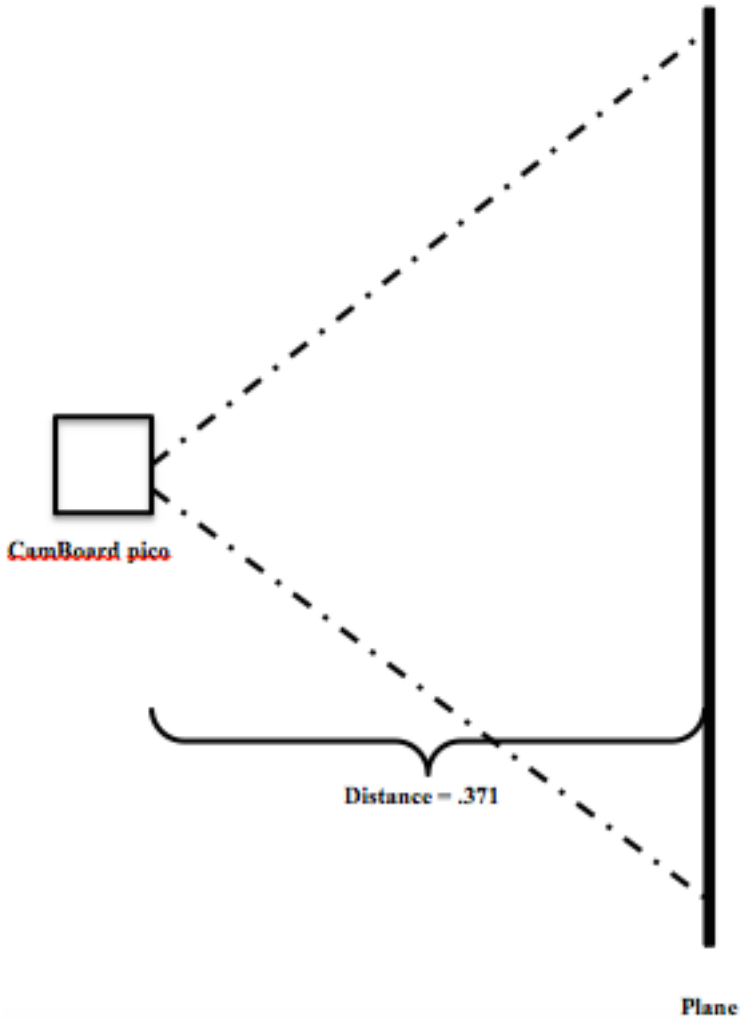

$$area\ in\ image = .256m^2$$

$$area\ of\ one\ pixel = \frac{area\ in\ image}{\#\ of\ pixels\ (120\times176)} = 9\times10^{-6}m^2$$

$$\frac{Energy}{count} = \frac{P_{peak} * t_{integration} * area\ of\ pixel * angle\ reflected\ into * distance^2}{\#counts}$$

$$\frac{Energy}{count} = 8.59\times10^{-16}\ J$$

$$\frac{photons}{pixel} = \frac{E}{count} * \frac{1}{E_{850}} = 3671\ photons$$

The typical path length of a photon through fatty tissues is on the order of 10cm. At a distance of .13 m to the flat plane, the number of photons incident to each pixel skyrockets to a little over 3671 photons/pixel. However, it is very important to note that if this system were being used with a diffusive material such as fat, a substantial portion of these photons would be lost.

We must also know the error of the device in determining distances from recorded phase differences. We must be able to see sufficiently small variations in the phase due to the different path lengths taken by the photons to arrive at the detector array of the camera. It is critical that we have statistical confidence that these variations are due to path difference, not instrumental variation or thermal noise.

Figure 10: Phase Image Showing location of Vertical Sample

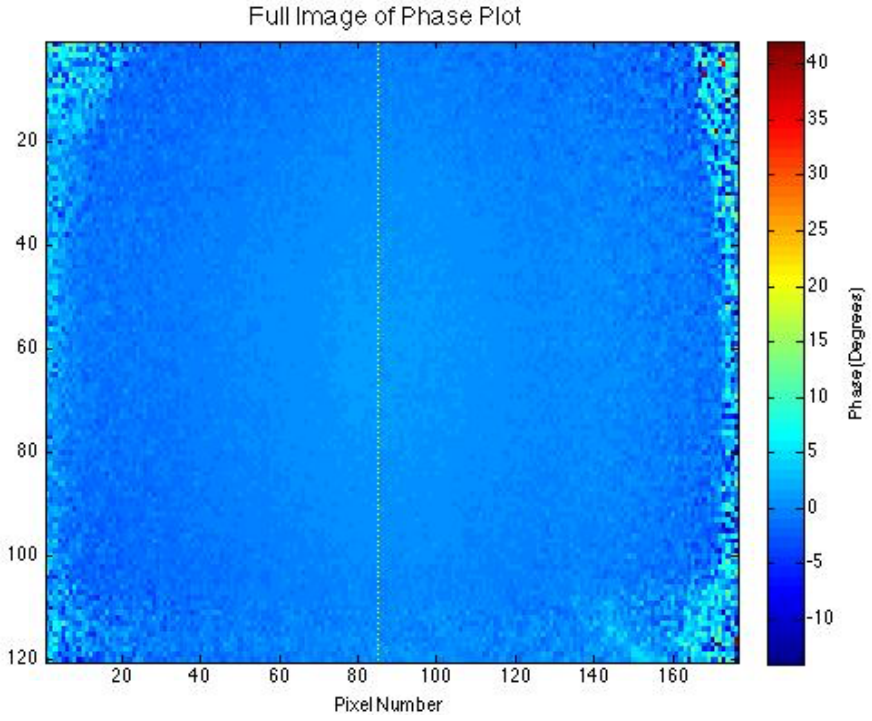

The figure is showing the full phase plot. The vertical line at column 85, designated by the yellow line, was chosen to model the phase as the distance from the center region (corresponding to the smallest phase shift and smallest distance traveled) changes.

Figure 11

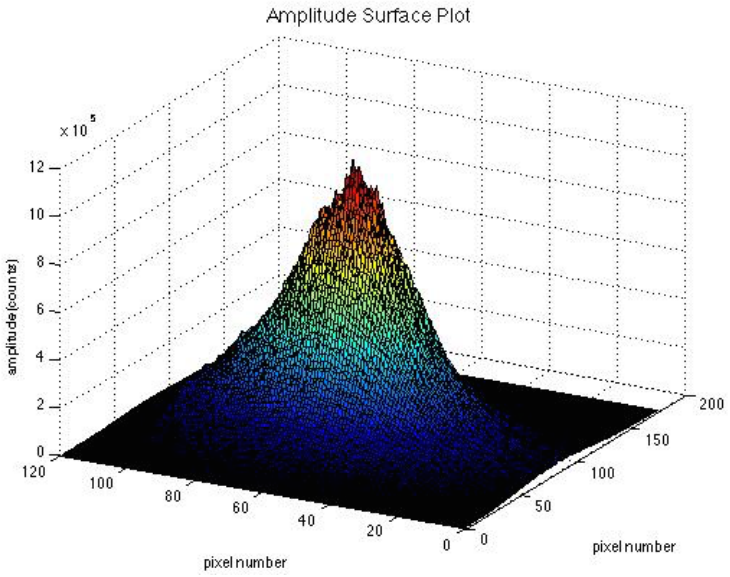

This image shows the 3-dimensional distribution of the amplitude at a distance of .3 cm away.

The phase was modeled by determining the angles and distances that corresponded to each 1 pixel increment from the location of highest intensity, row 65 (Figure 11). The relationship followed a linear trend with the following equations.

$$First\ part\ of\ model(1{:}\,65){:} \qquad y = .0004195x - .005$$
$$Second\ part\ of\ model(65{:}\,120){:} \qquad y = -.0005095x + .055$$

The second part of the model, from row 65 to 120, had considerably more noise toward the lower end (nearer to 120). This is likely because some of the light was hitting the table first and not striking the plane directly. The residuals were taken in these two sections of the fit (Figure 13). The average absolute value for the first was found to be .0027 rad. While in the second, it was found to be .0044 rad. According to the equation relating phase difference and distance,

$$d = \frac{c\phi}{4\pi f_m}$$

where c is the speed of light, f_m is the frequency of modulation, and ϕ is the phase difference, an uncertainty of .0027 rad would account for 2.1mm of uncertainty in the distance measurement.

Figure 12

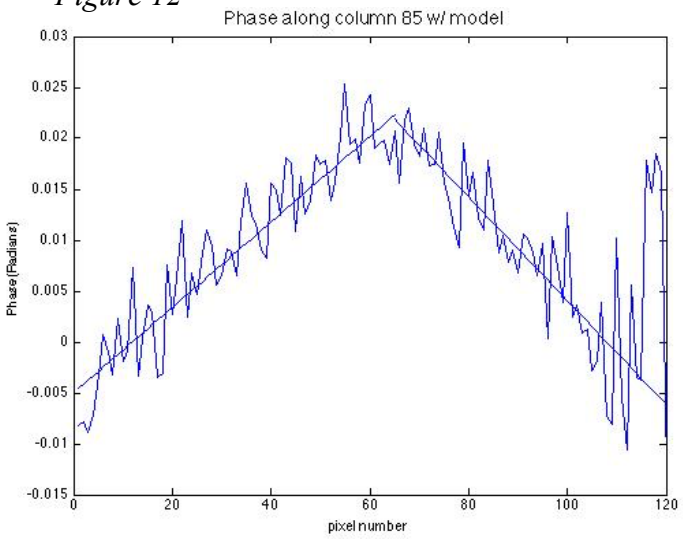

Figure 13

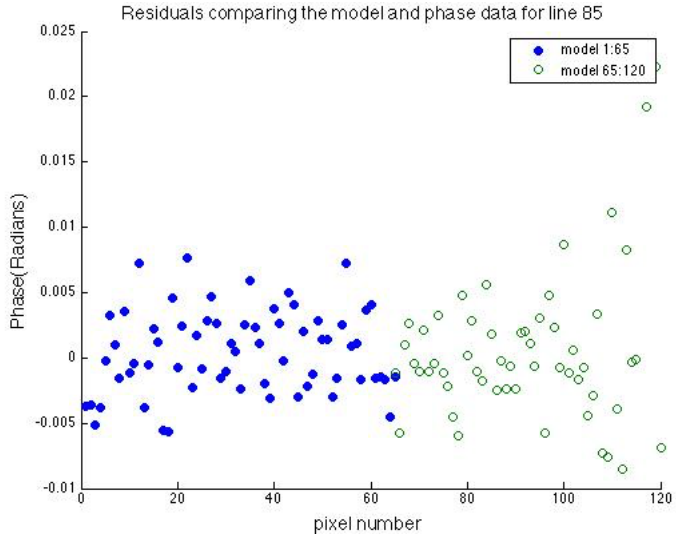

Conclusion

Because of the relatively robust signal strength of the camera without the aid of lenses (3671 photons incident to each pixel from .3m away) and small minimum discernable step size in the phase data (.0027 rad), lead me to conclude that this camera could be used as a powerful detector array for diffuse optical tomography. In addition, the small size and power supply needed would make for a compact, highly portable diffuse optical tomography system.

References

[1] D.A. Boas, D.H. Brooks, E.L. Miller, C.A. Dimarzio, M. Kilmer, R.J. Gaudette, Q. Zhang. "Imaging the Body with Diffuse Optical Tomography." IEEE Signal Processing Magazine, 57-75. Nov. 2001.

[2] Dehghani, H., Eames, M. E., Yalavarthy, P. K., Davis, S. C., Srinivasan, S., Carpenter, C. M., . . . Paulsen, K. D. (2008). Near infrared optical tomography using NIRFAST: Algorithm for numerical model and image reconstruction. Communications in Numerical Methods in Engineering, 25(6), 711–732. doi:10.1002/cnm.1162

[3] Eggebrecht, A. T., Culver, J. P. (2014). High-Density Diffuse Optical Tomography: Imaging Distributed Function and Networks in the Human Brain. Bio-Optics World, 7(4). Retrieved from http://www.bioopticsworld.com

[4] S.A. Prahl, "Optical absorption of hemoglobin," Oregon Medical Laser Center, OR, Tech. Rep., Dec. 15, 1999

[5] Reference Design Brief CamBoard Pico^{S} 71.19K" . Siegen, Germany: pmdtechnologies. 2014. Web. http://pmdtec.com/html/pdf/PMD_RD_Brief_CB_pico_71.19k_V0103.pdf.